

Kinematic vortex-antivortex lines in strongly driven superconducting stripes

G. R. Berdiyrov,¹ M. V. Milošević,¹ and F. M. Peeters^{1,2,*}

¹*Departement Fysica, Universiteit Antwerpen, Groenenborgerlaan 171, B-2020 Antwerpen, Belgium*

²*Departamento de Física, Universidade Federal do Ceará, Caixa Postal 6030, Campus do Pici, 60455-760 Fortaleza, Ceará, Brazil*

(Received 25 February 2009; published 6 May 2009)

In the framework of the time-dependent Ginzburg-Landau formalism, we study the “resistive” state of a submicron superconducting stripe in the presence of a longitudinal current. Sufficiently strong current leads to phase slippage between the leads, which is manifested as *oppositely charged kinematic vortices* moving in opposite directions perpendicular to applied drive. Depending on the distribution of superconducting current density the vortex-antivortex either nucleate in the middle of the stripe and are expelled laterally or enter on opposite sides of the sample and are driven together to annihilation. We distinguish between the two scenarios as a function of relevant parameters and show how the creation/annihilation point of the vortex-antivortex and their individual velocity can be manipulated by applied magnetic field and current.

DOI: 10.1103/PhysRevB.79.184506

PACS number(s): 74.78.-w, 73.23.-b, 74.40.+k, 85.25.-j

I. INTRODUCTION AND MODEL

Phase-slip phenomenon is already a long-known mechanism that allows superconductivity to survive in the presence of an electric field.¹ According to this scenario, in a narrow superconducting wire with applied longitudinal current the phase of the order parameter may periodically drop by 2π , virtually in a single point. In such points, called the phase-slip centers (PSC) the magnitude of the order parameter oscillates between zero and its maximum value. Analogously, the PSC may “grow” in a phase-slip line (PSL) in two-dimensional (2D) samples, even with width W much larger than the characteristic length scales² (see also Ref. 3 for review). Contrary to PSC, the oscillations of the order parameter may not necessarily be uniform along the PSL: these oscillations may occur in the form of propagating waves carrying the order parameter singularities across the sample. Such waves (named *kinematic vortices*) have been first observed in numerical simulations using the 2D time-dependent Ginzburg-Landau (TDGL) equations,⁴ and the experimental evidence for the existence of kinematic vortices was reported in Ref. 5.

However, topologically speaking, the condition of the phase-slippage over a PS line can be satisfied not just for a single kinematic vortex but also for *two singularities* propagating in opposite directions, i.e., a kinematic vortex-antivortex (V-Av) pair. Note that in the latter scenario the needed time for the PS process cuts to a half, compared to the kinematic vortex case. The main objective of the present paper is to discuss the conditions for either single- or two-species kinematic PSL as a function of the different parameters characterizing the superconducting sample. As an example, we consider a superconducting stripe driven into a nonequilibrium state by large electrical current where strong spatial variation of the condensate occurs and study the effect of size and position of the current leads, temperature, and applied (weak) magnetic field on the dynamics *within the phase-slip line*. Further we discuss the *repercussions* on the electronic properties of the stripe, e.g., the current-voltage (I - V) characteristics and output voltage vs time signal for a given current input.

Electric-field induced flux-flow instabilities have been studied in the past using TDGL theory.^{2,4,6-14} Although phenomenological in origin, this theory showed good agreement with the experiment both for one-dimensional (1D) (Refs. 9 and 10) and 2D (Refs. 11 and 12) superconductors. In the present paper, we consider a very thin (thickness $d \ll \xi, \lambda$) superconducting strip (length L , width W) generally in the presence of a perpendicular magnetic field and with a transport electric current applied through normal-metal leads (of size a , see Fig. 1). To explore the dynamic properties of the superconducting condensate in this system we used the TDGL equation in its generalized form^{15,16}

$$\frac{u}{\sqrt{1 + \gamma^2 |\psi|^2}} \left(\frac{\partial}{\partial t} + i\varphi + \frac{\gamma^2}{2} \frac{\partial |\psi|^2}{\partial t} \right) \psi = (\nabla - i\mathbf{A})^2 \psi + (1 - |\psi|^2) \psi. \quad (1)$$

This equation is coupled with the equation for the electrostatic potential $\Delta\varphi = \text{div}\{\mathcal{J}[\Psi^*(\nabla - i\mathbf{A})\Psi]\}$. In above equations, distances are expressed in units of coherence length, time is scaled by so-called GL time $\tau_{\text{GL}} = \pi\hbar/8k_B T u$, the electrostatic potential φ by $\varphi_0 = \hbar/2e\tau_{\text{GL}}$, and vector potential \mathbf{A} by $H_{c2}\xi$. Generalization of the usual TDGL theory comes from the parameter $\gamma = 2\tau_E\Psi_0/\hbar$, which characterizes the chosen material (with τ_E being the inelastic electron-collision time) and the term coupled to γ related to the relaxation (and

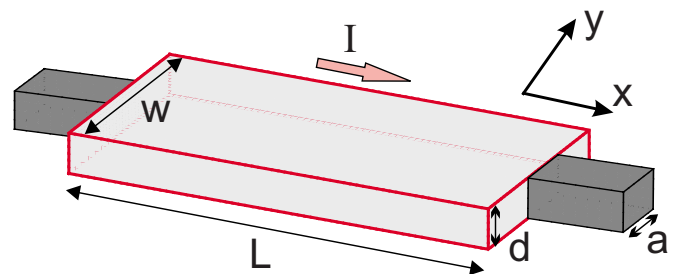


FIG. 1. (Color online) Schematic view of the sample—a superconducting sample (width W , length L , and thickness d) with attached normal leads (size a).

viscosity) of the condensate. In the present simulations, the coherence length and the penetration depth at zero temperature are taken as $\xi=10$ nm and $\lambda=200$ nm, which are typical values for thin Nb films.¹⁷ Using the normal-state resistivity $\rho=18.7 \mu\Omega$ cm for such films we obtain $\tau_{GL} \approx 6.72$ ps. Microscopically determined parameter $\mu=5.79$ is a suitable value for most low- T_c materials¹⁵ and we assumed $\gamma=20$ for the considered sample. Superconductor-vacuum boundary conditions $(\nabla - i\mathbf{A})\psi|_n=0$, $\nabla\varphi|_n=0$ are taken at all boundaries of the sample, except at the interface with current contacts where normal-metal-superconductor boundary conditions $\psi=0$ and $\nabla\varphi|_n=-j$ are used.

Since we work very close to T_c heating effects are not taken into account in our simulations. In this range of temperature the effect of heat dissipation becomes small.¹⁸ At low temperatures one should combine the GL equations with the heat diffusion equation¹⁹ to take into account the heat dissipation. However, recent numerical simulations^{10,12} showed that heating effects do not lead to qualitative changes in the dynamics of the superconducting condensate.

II. TRANSPORT PROPERTIES AND KINEMATIC VORTEX-ANTIVORTEX PAIRS

The calculated current-voltage characteristics of the sample with $L=600$ nm and $W=400$ nm at $T=0.96T_c$ is shown in Fig. 2(a) for two sizes of the current leads (a). The case $a=W$ (dashed curve) leads to an approximate uniform current distribution and the stripe is fully superconducting up to its first threshold current $I_{c1}=51 \mu\text{A}$.³⁰ At this current the superconducting current density $\mathbf{j}_s = \mathcal{J}(\Psi^* \nabla \Psi) - |\Psi|^2 \mathbf{A}$ exceeds locally the pair-breaking current j_{GL} and the system is driven into a nonequilibrium state.²⁰ This results in a jump and a change of the slope of the I - V curve, i.e., an abrupt switching of the sample into a state of higher electric resistivity.^{6,21–23} This state is characterized by the PSL solution whose nature is *independent* of W ; there the order parameter is strongly suppressed across a line that is situated at $x=L/2$, and vanishes periodically in time along the PSL perpendicular to the direction of the applied current flow. The second type of a dissipative phase-slip state [the vortex “street” (VS) solution] is characterized by the motion of real vortices (singularities with encircling 2π change of phase) perpendicular to the direction of the current, which is not obtained for this small width of the sample and chosen γ parameter.² With further increasing current, the system transits into a normal state (superconductivity is destroyed) at the second (real) critical current of $I_{c2} \approx 91 \mu\text{A}$.

For smaller leads (i.e., more locally injected current) the electronic instability of the condensate starts at smaller applied current [$I_{c1}=38 \mu\text{A}$, leading to a step in the I - V curve, see Fig. 2(a)]. The reason is the strongly nonuniform distribution of the transport current across the sample. As the applied current increases the current density reaches the depairing current density *in the middle* of the sample and the pair-breaking process leads to a prompt decrease in the order parameter in the very center of the stripe. As a consequence, a different kind of dissipative solution is obtained, compared to the case of uniform current (large a): V-Av pair nucleates

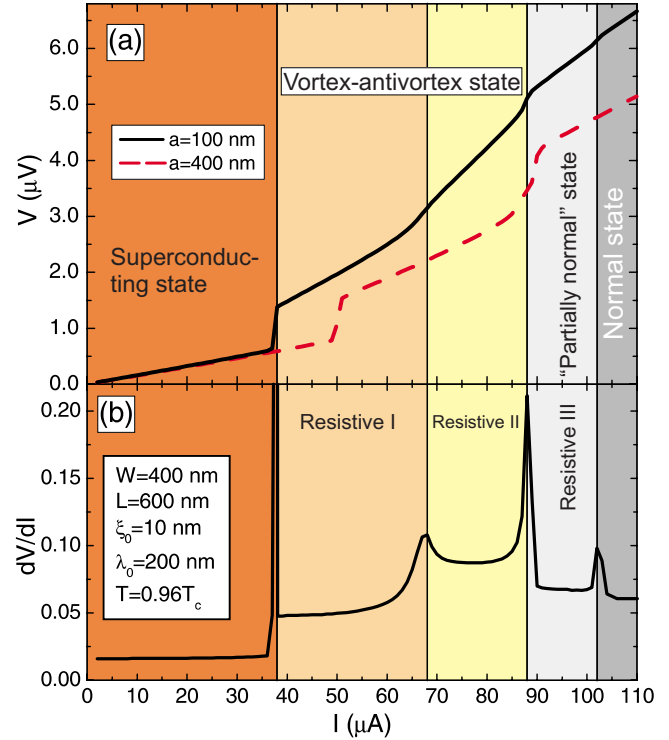


FIG. 2. (Color online) (a) Current-voltage (I - V) characteristics (obtained in increasing current regime) of a superconducting stripe of width $W=400$ nm and length $L=600$ nm connected to normal contacts with width $a=100$ nm (solid curve) and $a=400$ nm (dashed curve). The temperature is $T=0.96T_c$. The inset shows the schematic view of the sample. (b) The differential resistance dV/dI of the sample as a function of applied current for $a=100$ nm.

in the weak point of the sample. To demonstrate the creation, motion, and disappearance (i.e., leaving of the sample) of the V-Av pair, we plotted the order parameter along their line of motion in Fig. 3(a) for different time intervals. To emphasize once more, V-Av pair nucleates in the middle of the sample (curve 2) and is separated in opposite directions (lines 3–5) under influence of Lorentz force toward the lateral edges of the sample [see also contour plots in Fig. 3(a)]. After the expulsion, a new pair is created again in the middle of the sample, continuing the ever kinematic process. This periodic nucleation and motion leads to persisting oscillations of the voltage measured along the sample. Quite naturally, with increasing the applied current the speed of this process increases but no more than one V-Av pair at a time was found in the vortex channel for the considered parameters of the sample.

The latter dynamic behavior persists up to a current of $I=69 \mu\text{A}$, where a unique phenomenon is observed—with increasing the applied current, the I - V curve increases its slope but without a step in voltage. Consequently, the differential resistance dV/dI of the sample increases abruptly at this point [see Fig. 2(b)]. The snapshots of the order-parameter profile across the kinematic line [see Fig. 3(b)] show that the system transits into a *different* V-Av state: vortex and antivortex are now created on the opposite sides of the stripe [curve 1 in Fig. 3(a)], then move toward each other (curves 2–4) and annihilate in the middle of the sample

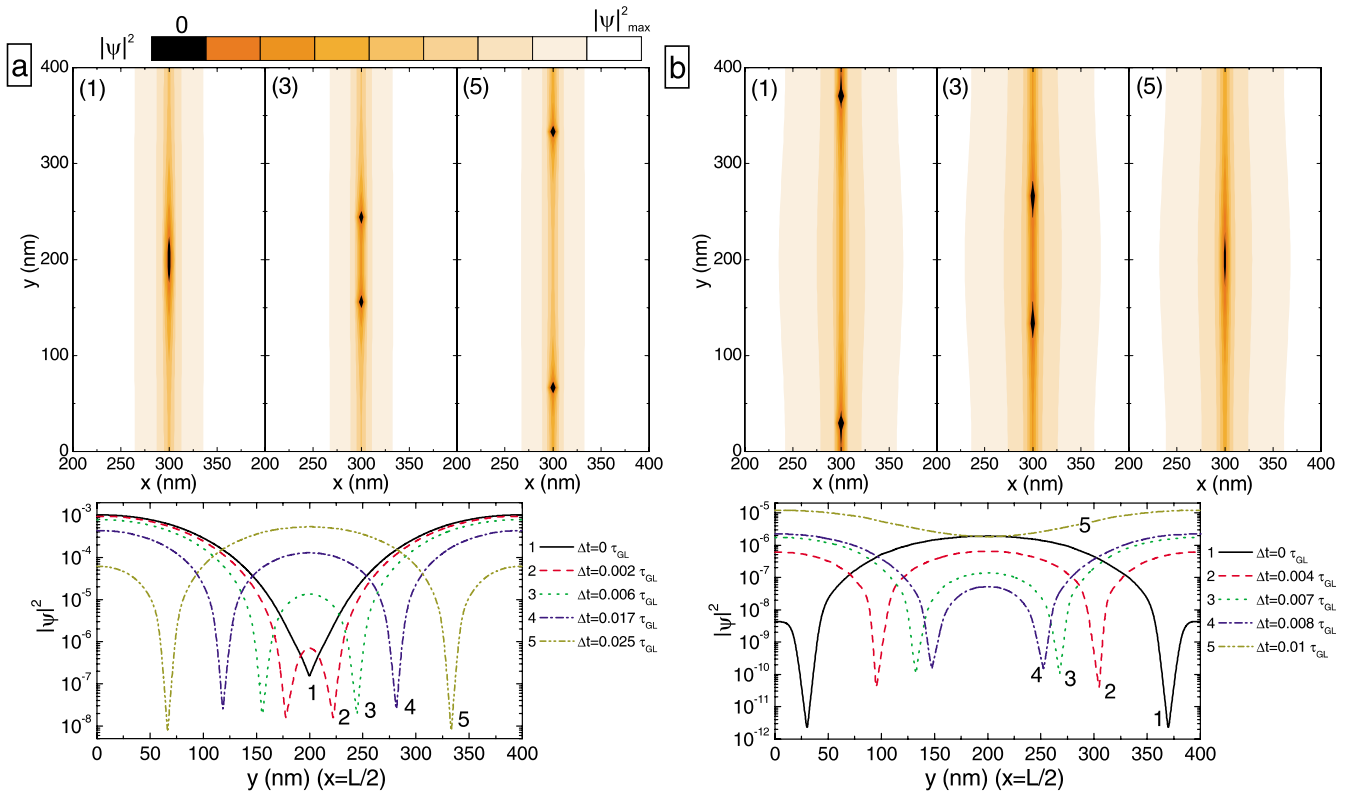


FIG. 3. (Color online) Lower parts of (a) and (b) are cross sections of the Cooper-pair density in the middle of the sample ($x=L/2$) at different times for the applied currents (a) $I=40 \mu\text{A}$ and (b) $I=72 \mu\text{A}$. The contour plots are snapshots of the Cooper-pair density at time intervals indicated in the main panels.

(curve 5). Note that after annihilation the new pair is not created at the point of annihilation but again at the sample edges, contrary to the predictions of Ref. 2. This is an important difference, proving the nonsolitonic nature of V-Av singularities, i.e., their annihilation/creation process cannot be described as a passage of two solitons through each other.

Going back to the I - V curve, we can now identify two distinct regions, the “Resistive I” (RI) and “Resistive II” (RII) state. In both cases we have the kinematic V-Av solution but with different dynamics of the V-Av pairs and with different rate of dissipation. Beyond the RII state, the system evolves into a resistive state where kinematics across the phase-slip line is lost—instead, a normal path is formed across the sample with no oscillation of the order parameter. Such “partially normal” (RIII) state is followed by the normal state at the critical current $I_{c2} \approx 102 \mu\text{A}$, where superconductivity is suppressed over the whole sample. Note that I_{c2} is significantly larger than the one found for the $a=W$ case.

At this point, we must address yet another interesting phenomenon—the behavior of differential resistance as a function of current [Fig. 2(b)]. We observed a unique manifestation of the negative differential resistance (NDR), one of the most fascinating effects in mesoscopic physics (see Ref. 24 and references therein). With increasing dc, the resistance of the sample increases over both kinematic V-Av states but then decreases over the partially normal state, finally to the normal-state resistance. It is not only remarkable that the NDR takes place but we also find that the resistance of the

RII and RIII states *exceed the normal-state resistance*. There is an obvious link between these resistance levels and phase-slippage, and we believe that this resistance anomaly results from the presence of a normal-superconducting (N-S) interfaces along the sample and near the I - V leads. The quasiparticles and Cooper pairs have different electrochemical potentials within the nonequilibrium regions, which extend over the distance λ_Q (the charge imbalance) around the N-S interface (i.e., the phase-slip line in our case). This results in increased resistance for quasiparticles in regions near to N-S interfaces (where their chemical potential linearly increases toward Cooper-pair value), as observed in the resistive measurements in thin Al films with regions of different transition temperatures.²⁵

As noted before, the appearance of kinematic V-Av lines in our sample is a consequence of the inhomogeneous distribution of current across the sample, enhanced by the smaller size of the current leads compared to the size of the sample. Nevertheless, these findings do depend on the dimensions of the sample and on the parameter γ . Namely, V-Av solution can be obtained even for the case of $a=W$ but in significantly larger samples ($W > 80\xi$). Moreover, latter threshold size of the sample for appearance of V-Av state *increases further* with increasing γ (Ref. 2) and goes beyond mesoscopic regime for materials like Al, where $\gamma \approx 1000$. Thus, in truly mesoscopic samples, here reported phenomena can only be seen for nanopatterned current leads on the sample. Following this conclusion, in what follows we analyze the distribution of locally injected current in the sample, in order to

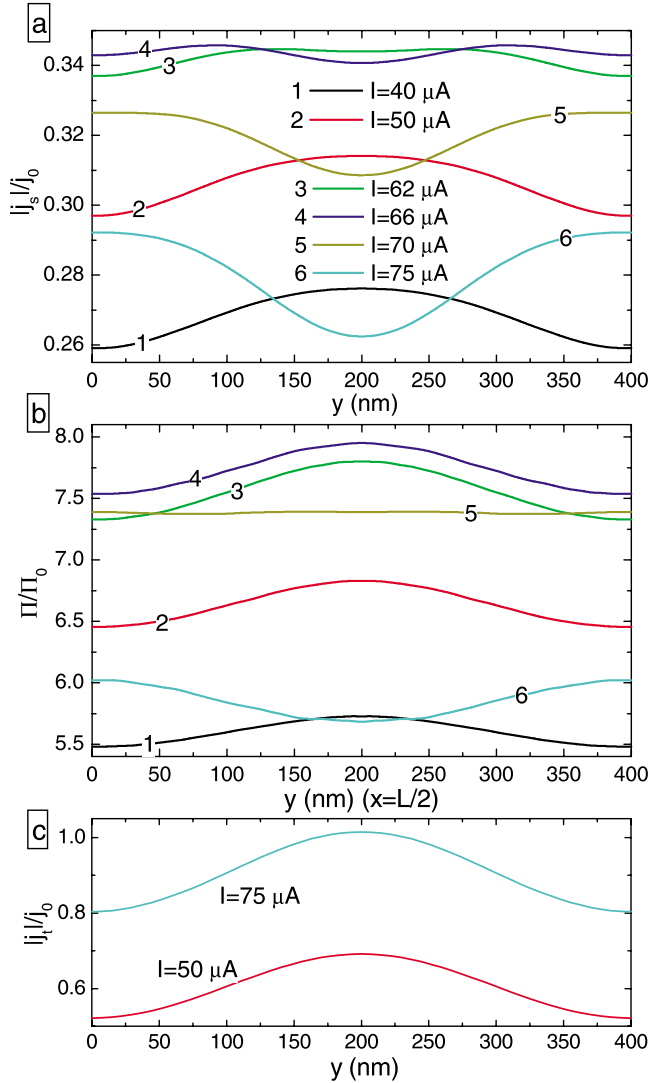


FIG. 4. (Color online) (a) Distribution of the time and length-averaged superconducting current density j_s (in units of $j_0 = cH_{c2}\xi/4\pi\lambda^2$) and (b) supercurrent velocity of the superconducting condensate $\Pi(x=L/2)$ (in units of $\Pi_0 = \xi H_{c2}$) across the width of the sample at zero-applied field and for different values of the applied current I . (c) The total current density j_t distribution over the width of the sample for two values of the applied current.

understand the origin of RI to RII transition. Figure 4(a) shows the distribution of the time-averaged supercurrent density $|j_s|$ over the width of the sample for different values of the applied current. Because of the inhomogeneous profile of the injected current for $a < W$, the supercurrent is maximal in the middle of the sample (line connecting the leads) and reaches the critical value at $I = 38 \mu\text{A}$, causing the nucleation of a V-Av pair. After this event j_s decreases but its distribution remains qualitatively unchanged (see curve 1). With increasing applied current, j_s increases (curve 2) and reaches the critical value beyond which it starts decreasing again (compare curves 3 and 4). Simultaneously, the profile of j_s changes as it decreases faster in the middle of the sample than at the edges (curve 3) and starting from $I = 69 \mu\text{A}$ the density of superconducting currents are clearly maximal at the edges of the sample (curves 5 and 6). This is

exactly where the transition from the RI state to the RII state takes place. Therefore, the distribution of supercurrents directly determines the nucleation point of the kinematic V-Av pairs. We would like to mention that, although the supercurrent density decreases with increasing the applied current I after the RI-RII transition [compare curves 5 and 6 in Fig. 4(a)] the total current $j_t = j_s + j_{\text{normal}}$ always increases with increasing I [see Fig. 4(c)].

Previous GL studies (see, e.g., Ref. 26) have shown that a weak point for the entrance of vortices is a position in space where the kinematic momentum (also called supervelocity) of the condensate is maximum. The latter is defined as $\Pi = |(\nabla\theta - \mathbf{A})|$, with θ the phase of the order parameter. Figure 4(b) shows the distribution of the supervelocity Π across the sample along the vortex street just before the appearance of V-Av pairs. At smaller currents supervelocity exhibits a maximum in the middle of the sample, where V-Av pairs are created (curve 1–4). Close to the RI/RII state transition Π becomes more uniform and immediately after this transition the maximum shifts to the edges of the sample (curve 6). As we will show in Sec. III, the spatial maximum of the supervelocity predetermines the V-Av nucleation point.

III. INFLUENCE OF APPLIED MAGNETIC FIELD ON THE KINEMATIC VORTEX-ANTIVORTEX DYNAMICS

In this section, we demonstrate the effect of the applied magnetic field H on the dynamics of kinematic V-Av pairs in the sample (same parameters used as in Fig. 2, i.e., $a = 100 \text{ nm}$). Simulations are done in zero-field cooling regime, i.e., we started from fully superconducting state ($|\psi|^2 = 1$) and applied a magnetic field H . The external current is applied after the stationary solution is reached. We restrict ourselves to a weak magnetic-field regime so that *no Abrikosov vortices* enter the sample in the absence of applied current. In such conditions, the qualitative form of the I - V characteristics does not change and RI and RII kinematic states are still present. We find that applied perpendicular magnetic field influences the creation (in RI region) and annihilation point of V-Av pairs (in RII region): both of them shift away from the center of the sample [see Figs. 5(a) and 5(b)], in the direction that favors longer presence of the vortex in the sample (and vice versa for the antivortex). The reason behind this shift lies in the Meissner currents, which are induced to screen the applied magnetic field and which are maximal near the lateral edges. As a result, the total supercurrent becomes more nonuniform leading to the drift of the nucleation/annihilation (N/A) point. The exact position of V-Av creation and annihilation is determined by the maximum of the supervelocity, which is shown in Fig. 6(a) for the applied field $H = 2 \text{ Oe}$. Note that Π profiles in Fig. 6(a) are normalized to $0 \rightarrow 1$ scale for clarity [calculated Π values strongly depend on the applied current value, see Fig. 4(b)]. The effect of magnetic field is particularly pronounced for applied currents near the RI/RII transition, where N/A points evidently shift closer toward the edges of the sample [see Fig. 5(b) and curve 2 in Fig. 6(a)]. Moreover, there exists a region [shaded area in Fig. 5(b)] where *only a kinematic*

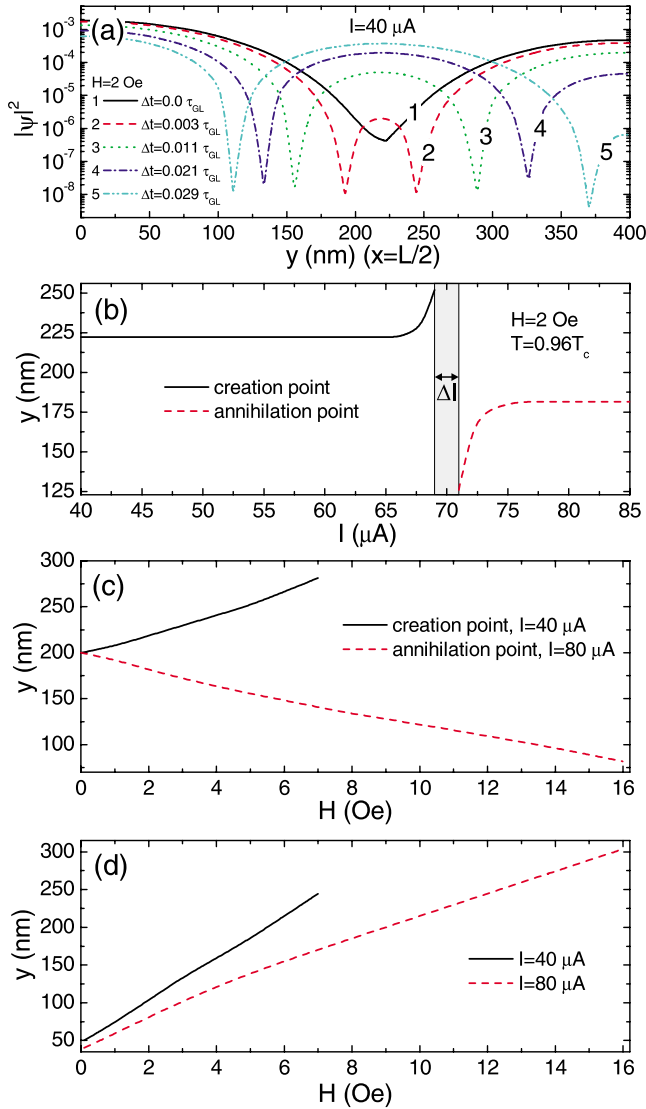


FIG. 5. (Color online) (a) The cross sections of the Cooper-pair density in the middle of the sample ($x=L/2$) at different times for $I=40 \mu\text{A}$ and $H=2 \text{ Oe}$. (b) Dependence of the creation (solid curve) and annihilation (dashed curve) points of the V-Av pair on the applied current for $H=2 \text{ Oe}$. (c) Creation (solid curve) and annihilation (dashed curve) points as a function of applied field for $I=40 \mu\text{A}$ and $I=80 \mu\text{A}$. (d) The distance that vortex travels across the sample before the creation of the antivortex at the opposite edge of the sample as a function of applied field H for $I=80 \mu\text{A}$.

vortex is nucleated at the top edge of the sample and travels to the opposite edge (without the corresponding antivortex) but still provides for persisting oscillations of the voltage similar to the kinematic V-Av case. In this region the super-velocity is maximum at the edge of the sample [curve 3 in Fig. 6(a)]. The area of such single-species kinematic line increases with increasing applied field (as latter further disfavors the appearance of an antivortex; e.g., $\Delta I=10 \mu\text{A}$ for $H=8 \text{ Oe}$).

Contrary to the results in absence of the applied field ($H=0$), in the RII state V-Av pair does not nucleate simultaneously; instead, the vortex nucleates first at the edge of the sample and moves under the action of Lorentz force (see Fig.

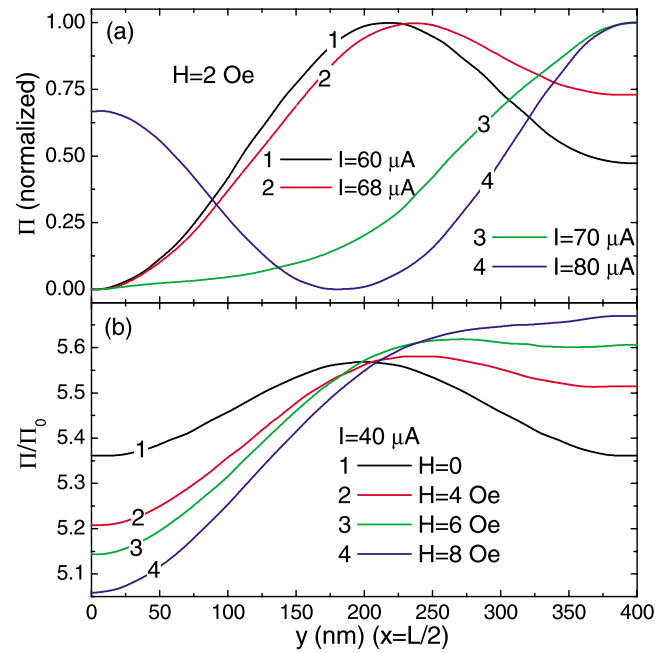


FIG. 6. (Color online) Supervelocity Π of the superconducting condensate across the sample ($x=L/2$) for (a) $H=2 \text{ Oe}$ (Π is normalized to $0 \rightarrow 1$ scale) and different values of the applied current I and for (b) $I=40 \mu\text{A}$ and different values of magnetic field.

7). Figure 5(d) shows the distance that vortex travels without the antivortex in both RI and RII regimes. Somewhat later, the antivortex appears at the opposite site of the sample and moves toward the annihilation with the vortex. This effect is explained by the difference of the value of Π at different edges of the sample [curve 4 in Fig. 6(a)]. Now the annihilation point is defined by the minimum of Π distribution [curve 4 in Fig. 6(a)].

Figure 5(c) shows the extent to which one can shift the creation/annihilation point with increasing H for two values of applied current corresponding to the RI and RII state. Note that both curves in the figure do not reach the edges of the sample, i.e., the creation (annihilation) point cannot be shifted to the very edge of the sample in the RI (RII) regime. To explain this we plotted in Fig. 6(b) the supervelocity of the condensate for $I=40 \mu\text{A}$ and for different magnetic fields. With increasing the applied field the maximum in the Π distribution shifts toward the edge of the sample (curves 1–3) and at $H=8 \text{ Oe}$ this maximum suddenly jumps to the edge of the sample (curve 4), i.e., for larger magnetic fields no V-Av pair appears in the sample and only the kinematic vortex is found. This indicates that the transition from two-species to single-species kinematic lines as a function of magnetic field is of first order. It is also worth noting that the creation point in RI state is more easily pushed out from the sample by magnetic field than it is the case with the annihilation point in the RII state [for chosen currents in Fig. 5(c), the found expulsion fields for N/A points are 7/16 Oe, respectively]. Consequently the distance that vortex passes without the antivortex is larger in the RI regime [Fig. 5(d)]. This asymmetry in the shift of nucleation and annihilation point follows from their position with respect to the distribution of supercurrents in the sample. Namely, the creation

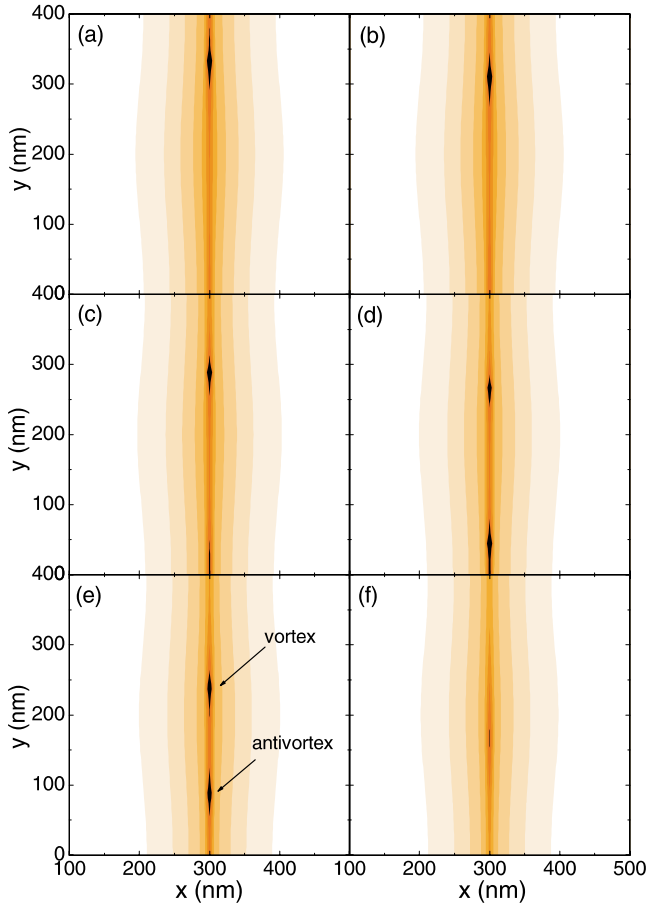


FIG. 7. (Color online) The contour plots of the Cooper pair density at time intervals: (a) $\Delta t=0\tau_{GL}$, (b) $\Delta t=0.005\tau_{GL}$, (c) $\Delta t=0.01\tau_{GL}$, (d) $\Delta t=0.015\tau_{GL}$, (e) $\Delta t=0.02\tau_{GL}$, and (f) $\Delta t=0.03\tau_{GL}$. The applied current is $I=80\ \mu\text{A}$ and the applied field is $H=4\ \text{Oe}$. The same scale as in Fig. 3.

point lies in an area with maximal supercurrent, which is a superposition of the supercurrents due to the applied current and the Meissner current. The annihilation point is situated in the region where the latter two supercurrents cancel each other. Therefore, larger Meissner current, i.e., larger magnetic field is necessary to shift the annihilation point toward the edge of the sample. Since the Meissner current has a linear dependence on the applied field,²⁷ the nucleation/annihilation points for the kinematic vortices depend linearly on the magnetic-field strength.

IV. TUNING OF THE VORTEX AND ANTIVORTEX VELOCITY BY THE MAGNETIC FIELD

It is already known from the previous studies^{4,5} that kinematic vortices exhibit similarities with both Abrikosov and Josephson vortices and can have large velocity. Indeed, experiments on Sn samples⁵ showed that kinematic vortices can move along the vortex “street” with velocity $v_{kv} \approx 10^5\ \text{m/s}$, which is much larger than the maximal measured speed of Abrikosov vortices $v_{Av} \approx 10^3\ \text{m/s}$.²⁸ At the same time, v_{kv} is still much smaller than the characteristic velocity of Josephson vortices $v_{Jv} \approx 10^7\ \text{m/s}$. Still, the

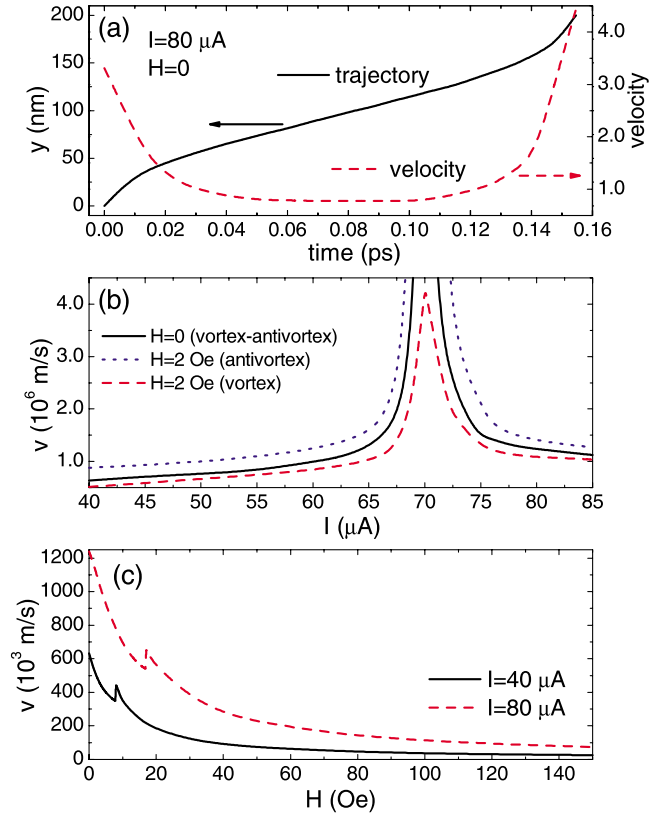


FIG. 8. (Color online) (a) The trajectory (solid curve and left axis) and the local velocity (dashed curve and right axis) of a vortex between the sample edge and the annihilation point (in the middle of the sample) for $H=0$ and $I=80\ \mu\text{A}$. (b) The average velocity of vortices and antivortices as a function of applied current at $H=0$ (solid) curve and $H=2\ \text{Oe}$ (dashed and dotted curves). (c) The dependence of average speed of vortices on the applied magnetic field for $I=40\ \mu\text{A}$ (solid curve) and $I=80\ \mu\text{A}$ (dashed curve).

model of kinematic vortices in Ref. 4 suggests that these vortices can move with *arbitrarily high velocity* depending on the value of the driving force and on the distribution of the current over the sample. In that picture, conventional phase-slip lines can be interpreted as kinematic vortices with infinite velocity.

However, the kinematic vortices do not move with constant speed over the sample, as they accelerate near the annihilation point and near the edges of the sample² [see Fig. 8(a) for the trajectory (solid curve) and the local velocity (dashed curve) of a vortex]. Therefore, we plotted in Fig. 8(b) the average velocity of the kinematic vortex (and antivortex) v as a function of applied current. As seen in this figure, for small current the vortex velocity increases almost linearly with the current I . For larger currents, close to RI/RII transition, v increases much faster. This tendency continues to divergency, i.e., transition to a phase-slip line, at the very RI/RII transition. Near this transition point the distribution of the supercurrents becomes virtually uniform across the sample [see, e.g., Fig. 4, curve 3]. Surprisingly, the velocity of V-Av pairs exhibits mirror-opposite behavior in the RII state, i.e., decreases with further increasing the applied current.

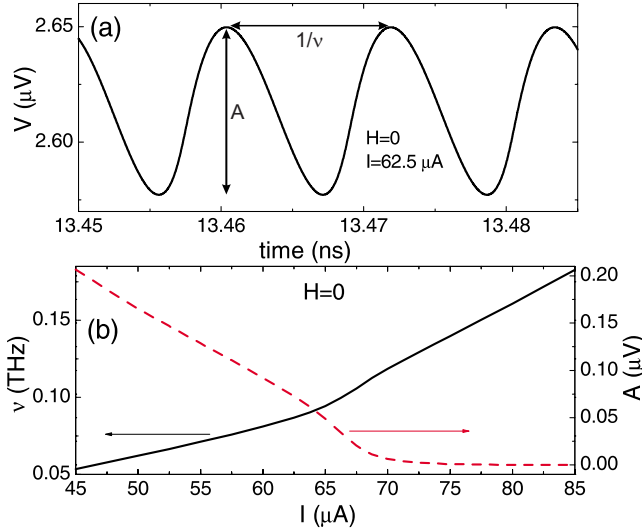


FIG. 9. (Color online) (a) The time evolution of the voltage for $I=62.5 \mu\text{A}$ and (b) the frequency (solid curve and right axis) and amplitude (dashed curve and left axis) of the instant voltage as a function of applied current I . The applied magnetic field is $H=0$.

Dashed curves in Fig. 8(b) show the influence of a weak positive magnetic field ($H=2 \text{ Oe}$). As shown there, applied positive field *increases* the speed of antivortices and *decreases* the speed of vortices. As we discussed above, there is

a ΔI gap where only vortices appear in the sample. Figure 8(c) shows the magnetic-field dependence of just the vortex speed (antivortex not shown) for two values of applied current. $v(H)$ function has a jump which characterizes the disappearance of antivortices in the sample, i.e., only a vortex travels across the sample. The velocity exhibits a $1/H$ background dependence and for larger H it approaches the value obtained before for conventional Abrikosov vortices.

Up to now we presented the time-averaged voltage at the contacts. But because of the presence of moving vortices (and antivortices) this voltage oscillates in time, which will result in the emission of electromagnetic radiation. In Fig. 9(a) we show the $V(t)$ curve for applied current $I=62.5 \mu\text{A}$ and no applied magnetic field. Although a trivial conclusion is that maxima/minima of the voltage correspond to the nucleation and annihilation of V-Av pairs, the situation turns out to be very different. The lifetime of V-Av pairs is actually *much smaller than the period of shown voltage oscillations* [compare time scales in Fig. 8(a) and in Fig. 9(a)]. The latter can be explained by Larkin and Ovchinnikov theory,²⁰ according to which the energetic distribution of the quasiparticles in the normal core of the vortex changes at high vortex velocities. Qualitatively, when the vortex passes through a given location, the spectrum of quasiparticles must switch rapidly from the superconducting branch to the normal branch. Due to the finite inelastic-scattering time τ_E , the switching process does not take place instantaneously. As a result the removal of the normal excitations from the vortex core takes place and the core of the vortex shrinks. The distribution function of quasiparticles changes in such a way that the number of quasiparticles in front of the vortex is less

than the equilibrium value and larger behind the vortex. Therefore, the system needs a finite time to recover superconductivity. However, for larger applied magnetic fields the speed of a kinematic vortex decreases [see Fig. 8(c)] and the minimum (maximum) of the voltage oscillations correspond to the entry (exit) of the kinematic vortex.

With view on future experiments, in Fig. 9(b) we summarize the measured amplitude (dashed curve and right axis) and frequency (solid curve and left axis) of the voltage as a function of applied current I . Note that with increasing the applied current the frequency of the oscillations increases. Therefore, for somewhat different geometrical parameters of the sample, frequency of the measured voltage oscillations can easily be tuned into the THz gap.²⁹

V. CONCLUSIONS

In summary, using the time-dependent Ginzburg-Landau formalism, we studied the transport properties of thin superconducting stripes with attached normal leads in the presence of a perpendicular magnetic field. We found that depending on the parameters of the sample the resistive state is represented either by a phase-slip line, which is the 2D analog of the 1D phase-slip center, or by the vortex “street” solution, which is characterized by a fast moving vortex singularity across the sample. In the latter case, and for narrow leads for injection of the current, we found that the kinematic vortices actually nucleate as *vortex-antivortex pairs* in the middle of the sample, where the supercurrent density j_s is maximal, and move perpendicular to the direction of the drive. When the distribution of j_s changes (at higher driving currents), V-Av pairs nucleate at the edges of the sample and move toward the center of the sample where they annihilate (prior to their periodic reappearance). These two scenarios result in different differential resistance of the sample. The position of creation/annihilation points in both scenarios can be manipulated by applied (weak) magnetic field to the point that only kinematic vortices remain in the sample (thus a transition from two-species to a single-species kinematic line is induced).

The distribution of the current across the sample is most influential on the velocity of the kinematic vortex-antivortex pair—the more uniform the current distribution, the faster the (anti)vortices move. In principle, (anti)vortex velocity can be tuned by applied current to an arbitrary value, where infinite velocity corresponds to a conventional phase-slip line. The speed of the kinematic (anti)vortex is also influenced by magnetic field, in a way that positive field slows down the vortex but propels the antivortex. At the same time, vortex velocity is inversely proportional to the applied field, converging to the velocity of the Abrikosov vortex for large applied fields. We envisage the applicability of such highly tunable position and velocity of the kinematic vortex-antivortex in devices requiring time-dependent source of bipolar magnetic field (with tunable distance between poles) but also in futuristic THz devices, as we found that the voltage across the sample in the kinematic phase can easily exhibit oscillations with THz frequency.

Of course, the findings of the paper depend on the parameters of the sample. For example, the speed of the kinematic vortices and consequently the frequency of the voltage oscillations increases with decreasing the width of the sample. For longer samples, the number of vortex streets (quasiphase slip lines) increase^{5,14} and the motion of kinematic vortices in neighboring vortex streets are out of phase. At larger mag-

netic fields such quasiphase slip lines coexist with slow moving vortices between such lines.¹³

This work was supported by the Flemish Science Foundation (FWO-VI), the Brazilian Science Foundation CNPq, and the Belgian Science Policy (IAP). G.R.B. acknowledges support from FWO-Vlaanderen.

*francois.peeters@ua.ac.be

- ¹B. I. Ivlev and N. B. Kopnin, *Usp. Fiz. Nauk* **142**, 435 (1984) [*Sov. Phys. Usp.* **27**, 206 (1984)].
- ²A. Weber and L. Kramer, *J. Low Temp. Phys.* **84**, 289 (1991).
- ³I. M. Dmitrenko, *Low Temp. Phys.* **22**, 648 (1996).
- ⁴A. Andronov, I. Gordion, V. Kurin, I. Nefedov, and I. Shereshevsky, *Physica C* **213**, 193 (1993).
- ⁵A. G. Sivakov, A. M. Glukhov, A. N. Omelyanchouk, Y. Koval, P. Muller, and A. V. Ustinov, *Phys. Rev. Lett.* **91**, 267001 (2003).
- ⁶W. Klein, R. P. Huebener, S. Gauss, and J. Parisi, *J. Low Temp. Phys.* **61**, 413 (1985).
- ⁷I. S. Aranson, L. Kramer, and A. Weber, *J. Low Temp. Phys.* **89**, 859 (1992); I. Aranson, M. Gitterman, and B. Ya. Shapiro, *ibid.* **97**, 215 (1994).
- ⁸M. Machida and H. Kaburaki, *Phys. Rev. Lett.* **71**, 3206 (1993).
- ⁹D. Y. Vodolazov, F. M. Peeters, L. Piraux, S. Mátéfi-Tempfli, and S. Michotte, *Phys. Rev. Lett.* **91**, 157001 (2003).
- ¹⁰A. K. Elmurodov, F. M. Peeters, D. Y. Vodolazov, S. Michotte, S. Adam, F. de Menten de Horne, L. Piraux, D. Lucot, and D. Maily, *Phys. Rev. B* **78**, 214519 (2008).
- ¹¹I. V. Grigorieva, A. K. Geim, S. V. Dubonos, K. S. Novoselov, D. Y. Vodolazov, F. M. Peeters, P. H. Kes, and M. Hesselberth, *Phys. Rev. Lett.* **92**, 237001 (2004).
- ¹²D. Y. Vodolazov, F. M. Peeters, M. Morelle, and V. V. Moshchalkov, *Phys. Rev. B* **71**, 184502 (2005).
- ¹³D. Y. Vodolazov and F. M. Peeters, *Phys. Rev. B* **76**, 014521 (2007).
- ¹⁴G. R. Berdiyrov, A. K. Elmurodov, D. Y. Vodolazov, and F. M. Peeters (to be published).
- ¹⁵L. Kramer and R. J. Watts-Tobin, *Phys. Rev. Lett.* **40**, 1041 (1978).
- ¹⁶R. J. Watts-Tobin, Y. Krähenbühl, and L. Kramer, *J. Low Temp. Phys.* **42**, 459 (1981).
- ¹⁷A. I. Gubin, K. S. Il'in, S. A. Vitusevich, M. Siegel, and N. Klein, *Phys. Rev. B* **72**, 064503 (2005).
- ¹⁸W. J. Skocpol, M. R. Beasley, and M. Tinkham, *J. Low Temp. Phys.* **16**, 145 (1974).
- ¹⁹A. V. Gurevich and R. G. Mints, *Rev. Mod. Phys.* **59**, 941 (1987).
- ²⁰A. I. Larkin and Yu. N. Ovchinnikov, *Zh. Eksp. Teor. Fiz.* **68**, 1915 (1975) [*Sov. Phys. JETP* **41**, 960 (1976)]; A. I. Larkin and Yu. N. Ovchinnikov, in *Nonequilibrium Superconductivity*, edited by D. N. Langenberg and A. I. Larkin (North-Holland, Amsterdam, 1986), p. 493.
- ²¹L. E. Musienko, I. M. Dmitrenko, and V. G. Volotskaya, *Pis'ma Zh. Eksp. Teor. Fiz.* **31**, 603 (1980) [*JETP Lett.* **31**, 567 (1980)].
- ²²D. Babic, J. Bentner, C. Surgers, and C. Strunk, *Phys. Rev. B* **69**, 092510 (2004).
- ²³M. Tian, J. Wang, J. S. Kurtz, Y. Liu, M. H. W. Chan, T. S. Mayer, and T. E. Mallouk, *Phys. Rev. B* **71**, 104521 (2005).
- ²⁴V. R. Misko, S. Savelev, A. L. Rakhmanov, and F. Nori, *Phys. Rev. Lett.* **96**, 127004 (2006).
- ²⁵Y. K. Kwong, K. Lin, P. J. Hakonen, M. S. Isaacson, and J. M. Parpia, *Phys. Rev. B* **44**, 462 (1991).
- ²⁶D. Y. Vodolazov, I. L. Maksimov, and E. H. Brandt, *Physica C* **384**, 211 (2003).
- ²⁷E. H. Brandt, *Phys. Rev. B* **46**, 8628 (1992).
- ²⁸M. Tinkham, *J. Low Temp. Phys.* **35**, 147 (1979).
- ²⁹G. P. Williams, *Rep. Prog. Phys.* **69**, 301 (2006).
- ³⁰The finite voltage observed for currents below I_{c1} is due to the normal contacts.